Chapter 4
Role of Co-surfactant
in Reduction of Energy Barrier

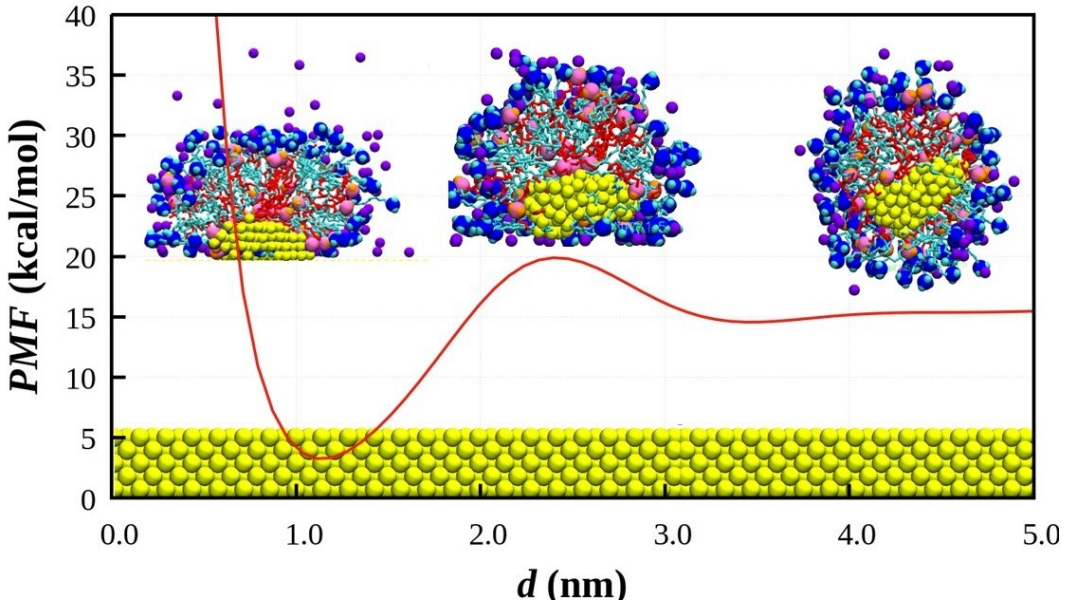

4.1 Introduction

Gold nanocrystals have gained immense interest in various fields due to their exceptional physical and chemical properties, allowing them to be tailored for specific applications in diverse fields such as catalysis,[3, 4, 157] optics,[114] sensors, [120, 121] electronics,[115–117] and manufacturing. [158] Their size- and shape-dependent optical,[41, 159] electrical[160] and catalytic[127] properties opened many avenues in biomedical applications[161], e.g. drug delivery [123–125], cancer treatment [129, 130, 132, 162], and bioimaging [128, 129] to advanced manufacturing,[163] electronics[118, 119] and environmental solutions.[164]

Several methods have been developed to synthesize nanoparticles with various sizes and shapes, requiring a deep understanding of the nucleation process in solution. Nucleation,

where a seed acts as a template for crystal growth, plays a crucial role in determining the nanoparticle morphology and size, influencing their electrical, optical, structural, and magnetic properties.[40, 48, 165] Across several decades, researchers explored different nucleation mechanisms, resulting in theories such as LaMer-Brust nucleation,[44] Oswald ripening,[45] Finke-Watzky nucleation,[46] coalescence and oriented attachment,[47, 166] etc. These classical models helped in explaining the thermodynamics behind nucleation. Generally, in all cases, pure metal nanocrystals begin nucleation slowly, followed by faster growth.[46] However, the growth is often extended till the last few atoms remain in the solutions. Hence, arresting the growth is also a key aspect of controlling the size and shape of the nanoparticles. Surfactants are pivotal in synthesising gold nanocrystals of different shapes and sizes, preventing undesirable growth and maintaining size uniformity. Surfactants, amphiphilic molecules, can adsorb onto the surface of growing nanocrystals, modifying atom attachment's surface energy and kinetics. They can direct the growth process by selectively binding to specific crystal facets, thereby controlling the shape, size and stability of the nanocrystals.[133, 140] Surfactants act as capping agents, providing a protective layer around growing nanocrystals and influencing nucleation and growth kinetics.[142, 167] Surfactants influence the nucleation stage by lowering the surface energy and stabilizing small clusters of atoms. This reduction in surface energy can significantly lower the nucleation barrier, facilitating the formation of nanocrystal seeds.[168]

When surfactants are added to an aqueous solution beyond the critical micelle concentration (CMC), surfactant molecules self-assemble into various structures, such as micelles[134], bilayers[137], rod-like[135], vesicles[136], and mesophases with various geometries.[138] Molecular dynamics (MD) simulations have been extensively used to characterize the equilibrium size, shape, hydration, and self-assembly of surfactants and co-surfactants.[70] The spontaneous aggregation of surfactant molecules, e.g. dodecylphosphocholine (DPC), can form worm-like micelles very quickly at high concentrations (0.46 M), whereas the formation of spherical micelles at lower concentrations (0.12 M) is found to be slower ($\sim$ 12 ns).[169] Different forcefields to describe molecular interactions showed considerable deviations for larger aggregates of surfactant molecules. Tang et al. used

GROMOS (three versions), CHARMM36, OPLS-AA, and OPLS-UA force fields to simulate preassembled micelles of various shapes (spherical, rodlike, bicelle) and sizes. Small micelles (aggregation numbers of 60 or 100) displayed minimal differences across force fields, whereas larger aggregates (e.g., 382 SDS molecules) exhibited significant structural variations.[170] When an aqueous solution of surfactants, e.g., SDS in water, is exposed to a surface like graphite, the surfactant molecules form self-aggregated structures – a hemispherical shape at lower concentration and cylindrical at a higher concentration.[34] Molecular dynamics simulations showed that surfactant molecules offer different degrees of ordering based on the nature of the interfaces.[68] However, in the presence of co-surfactant, the structure of the micelle and molecular ordering changes depending on the suitability of hydrocarbon tails.[69] A solvent-accessible surface area (SASA)-based method to understand and quantify micellization using histogram-reweighting Grand Canonical Monte Carlo (GCMC) simulations capable of accurately predicting CMC and micellar aggregation numbers.[71] The structure of the micelle and its structural evolutions played a critical role in the development of the nucleates inside the micelles.

The surface curvature played a crucial role in the growth mechanism of gold nanorods by facilitating ion diffusion. The intermicellar channels formed on curved surfaces are larger and more dynamic than those on any flat surfaces, allowing for easier migration of ions to the surface.[171] Surfactant-capped nanoparticles, e.g. CTAB-capped-Au Nanorods, were also engineered to form advanced functional materials using self-assembly of human serum albumin and the surfactants.[172] Many authors have utilized different ligands, such as thiols[173], amines[174, 175] and phosphines[176] as stabilizing agents to control key features of nanoparticles. The widely recognized Brust et al. method involves a two-phase synthesis of alkyl thiol-stabilized gold nanoparticles, resulting in particles that are soluble in organic solvents and have diameters of 5 nm or smaller with a relatively narrow size distribution.[173] Leff et al. later modified this approach by using amines as capping agents instead of thiols.[174] Further, Marchetti et al. have used the Leff method for synthesizing alkylamine-capped gold nanoparticles.[177] Perala et al. revealed a continuous capping and nucleation process in Brust-Schiffrin Synthesis (BSS) to prepare highly stable gold

nanoparticles.[178] However, a one-step synthesis of gold nanoparticles can be performed with the capping of oleylamine.[179] The use of mixed surfactants for the synthesis is not rare. Storm et al. investigated the solubilization using mixed micelles through molecular dynamics simulation and the COSMOmic model, revealing the structure, dynamics and solubilization capacity of micelles composed of different surfactants (Brij-35 and its mixture with CTAB or SDS).[180] Equimolar mixtures of linear and branched sodium dodecyl benzene-sulfonate (SDBS) surfactants showed different arrangements depending on the extent of coverage.[167] In addition, Kotsi et al. studied the behaviour of non-ionic (tristyrylphenol ethoxylates, EOT) and anionic (sodium benzene sulfonate, NaDDBS) surfactants in binary mixtures, with a lower critical micelle concentration (CMC) than NaDDBS, indicating their preference for adsorption at the water/air interface. Additionally, premixed surfactant systems took longer to equilibrate than surfactants added one by one, leading to lower equilibrium surface tension values and faster stabilization.[181] In a recent study, Suárez-López et al. investigated the synthesis of AuNPs through dissipative particle dynamics (DPD) simulations, focusing on the role of surfactants in the nucleation and growth of AuNPs.[182] Different types of surfactants, or the mixture of co-surfactants with primary surfactants, are still unexplored.

In this study, we present the effect of co-surfactant OLA on the nucleation and its growth on a surface, along with primary surfactant CTAB. While mixed surfactant systems such as SDS/CTAB or CTAB/Tween have been extensively investigated through both experiments and computations [183–186], there is limited molecular-scale insight into systems involving primary amine-based surfactants like OLA combined with conventional cationic surfactants. Our molecular dynamics simulation study presents, to the best of our knowledge, the first atomistic-level exploration of self-assembled structures of an OLA/CTAB system along with its adsorption behavior. Oleylamine (OLA), which consists of a long-chain unsaturated primary amine, interacts with co-surfactant CTAB via hydrophobic interactions between hydrocarbon chains and electrostatic interactions between the partially charged head groups.While CTAB molecules in aqueous solution form spherical micelles, the incorporation of a smaller number of OLA molecules to make it a stable cylindrical

micelle needs to be investigated on the molecular scale. How can cylindrical micelles be formed by tuning the OLA-to-CTAB molar ratio, highlighting the critical role of surfactant composition in controlling micelle shape and packing? This structural tunability is essential for enabling template-directed nanoparticle growth and enhancing surface-mediated nucleation processes. These simulations also reveal the sensitivity of micelle's shape and packing to the surfactants' molar ratio (OLA to CTAB ratio), a level of structural tunability crucial for applications in template-directed nanoparticle growth and surface-mediated nucleation processes. In this study, we present the effect of co-surfactant OLA on the nucleation and its growth on a surface, along with primary surfactant CTAB. The main reason for selecting OLA as a co-surfactant is its ability to alter the shape of the micelle from spherical to cylindrical, rod-like, or even elongated structures.[187, 188] This effect is due to the long hydrophobic tail of OLA, which can insert into the hydrophobic core of the micelle, increasing the volume of the core and causing structural changes. These changes can influence the nucleation of nanoparticles. When used in nanoparticle synthesis, OLA can play a dual role as a co-surfactant and stabilizer for nanocrystal formation, creating flexible environments that facilitate the nucleation and growth of gold nanocrystals. The cylindrical micelle, formed with CTAB and cosurfactant OLA, provides a confined space where the combination of hydrophobic interactions and structural heterogeneity directs the anisotropic growth of nanocrystals. OLA's influence on the growth of nanocrystals within the micelle, preventing aggregation and controlling particle size. The nucleation and growth of gold nanocrystals on a gold surface mediated by a CTAB micelle faced a steep energy barrier. [189] Potential of Mean Force (PMF) through umbrella sampling and WHAM indicated a more stable micelle in a bulk solution. As the micelle approached the surface, because of the strong layering of water molecules on the surface, it required a higher energy. Investigation of the structural properties of the micelle revealed the distortion of its structure during the process.

In this work, we present one method to reduce the structural rigidity and, hence, reduce the aforementioned energy barrier. This study provides important insights into the molecular mechanisms governing the nucleation and growth of gold nanocrystals on gold surfaces

and the subsequent role of a co-surfactant in engineering the micelle's structure. Additionally, the use of MD simulations allows us to quantify density profiles, radial distribution functions (RDF) and intermolecular interaction energies, providing mechanistic insights into the role of OLA in modifying the micelle structure and its adsorption behavior on gold surfaces. Previous experimental studies have shown that OLA can stabilize nanoparticles and direct anisotropic growth[190–192], but these do not capture the detailed molecular-level phenomena, which our simulation approach provides.

4.2 Models and Methodology

We have used molecular dynamics simulations to reveal the dynamics and structural aspects of the phenomenon. In this work, a mixture of OLA and CTAB (1:2) in water was used to prepare a mixed micelle in the aqueous phase. 80 molecules of CTAB and 40 molecules of OLA were distributed randomly in a simulation box containing 16000 water molecules. All the CH_3 and CH_2 groups were modelled as a united atom; all the nonbonded and bonded interactions between alike kinds were considered as per GROMOS96 53a6 forcefield.[93] The head groups, $–N(CH_3)_3$ and $–NH_2$ were modelled explicitly. An extended simple point charge (SPC/E) model was used to model water, the solvent. The charge on the CTA cation was such that the three methyl groups in the headgroup carried a partial positive charge of $0.1701e$, the methyl group adjacent to nitrogen carried a partial charge of $0.2167e$, and the methyl groups in the tail group were set to be neutral. The central nitrogen atom was set to be $0.273e$, and the bromide ions carry a charge of -1. The nitrogen atom in the amine group of co-surfactant OLA was set to be $-0.892e$, both the hydrogen atoms attached to the nitrogen in the amine group were set to be $0.356e$ each, the methyl group in the tail group of OLA was set to be $0.180e$, and rest groups in the OLA were set to be neutral. All the molecules were kept fully flexible. The nonbonded interactions between like and alike particles were modelled as per Lennard-Jones(12-6). The bond stretching and bending were described using harmonic potentials. For torsional interactions, a hybrid OPLS-style potential was employed to represent the NH_2-CH_2-CH_2-CH_2 and CH_2-CH_2-CH_2-CH_3 dihedral interactions, capturing

the multi-term periodic nature characteristic of such systems. Additionally, a quadratic potential was used to describe the CH_2-CH=CH-CH_2 torsional energy, suitable for planar or nearly planar configurations. All the interaction parameters used in this study are listed in Table 4.1. For nonbonded interactions, a cutoff distance of 12 was used. Long-range electrostatic interactions were calculated using the particle-particle particle-mesh (PPPM) method [193] with a real space cut-off of 1 nm, a grid spacing of 0.8 nm, and an interpolation order of 10^{-4}. The Lorentz-Berthelot mixing rule was employed to calculate non-bonded van der Waals interactions.[194, 195] Bonds and angles of a water molecule were constrained using the SHAKE algorithm.[100] All MD simulations were performed using LAMMPS software.[149] VMD[150] was used to visualize the simulation trajectories. The simulation box was considered periodic in all three directions. The temperature and pressure were maintained by the Nosé-Hoover thermostat (relaxation time is 0.2 ps) [102] and the Parrinello-Rahman barostat (relaxation time is 2.0 ps),[105] respectively. The evolutions of the systems were stored every 1 ps.

The mixture of the CTAB and OLA in water was allowed to evolve for 65 ns in an NPT ensemble to form a cylindrical micelle, which was used for further simulations. The gold surface was kept frozen by nullifying all the active forces. The aqueous solution was placed on the frozen gold surface and equilibrated for 2.0 ns in an NVT ensemble, keeping the temperature at 303.15 K. Molecular dynamics production runs were performed for 60 ns with a timestep of 2 fs to integrate the equation of motion using the Velocity Verlet algorithm.[89]

The formation of a cylindrical micelle comprising co-surfactant OLA and primary surfactant CTAB is illustrated in Figure 4.1. Figures 4.1(a) and (b) display the structural models of CTAB and OLA molecules, respectively. In these representations, the hydrophilic headgroups are denoted by black circles, while the hydrophobic tails are represented in cyan for CTAB and red for OLA. The simulation box, shown with a blue outline, was periodic in all three dimensions to mimic the behaviour of the bulk solution. We randomly distributed 100 gold atoms in the solution, allowing the formation of nucleates of varying sizes and shapes. The energy landscape for the fusion of nucleates with the gold surface

Table 4.1: Force Field Parameters for Oleylamine Molecules.

Nonbonded Interactions				
Atom	σ_{ij} **(Å)**	ϵ_{ij} **(kcal/mol)**	q **(e)**	
CH_3	3.75	0.194	0.0	
CH_2	3.95	0.091	0.180	
CH	3.73	0.093	0.0	
NH_2	3.34	0.2206	-0.892	
H	0.0	0.0	0.712	
Bond-stretching				
Bond	r_0 **(Å)**	k_b **[kcal/mol.Å^2]**		
N-CH_2	1.448	500		
CH_2-CH_3	1.535	500		
CH_2-CH_2	1.535	500		
CH=CH	1.33	500		
N-H	1.01	500		
Bending				
Angle	θ_0 **(Å)**	k_θ **[kcal/mol.Å^2]**		
H-N-H	106.4	87.205		
CH_2-CH_2-CH_2	109.5	334.72		
H-N-CH_2	109.5	200		
NH_2-CH_2-CH_2	119.7	139.85		
Torsion (kcal/mol)				
Dihedral	k_1	k_2	k_3	k_4
NH_2-CH_2-CH_2-CH_2	0.0	0.7055	-0.135	1.5727
CH_3-CH=CH-CH_2	49.25	-	-	-
CH_2-CH_2-CH_2-CH_3	0.0	0.7056	-0.1355	1.5727

was calculated using the umbrella sampling technique[155] followed by the Weighted Histogram Analysis Method (WHAM) [154]. In the umbrella sampling, a series of 70 linearly spaced windows along the reaction coordinate, defined by the distance between the centre of mass of the nucleate and the apex of the gold surface, were subjected to an external biasing potential to facilitate comprehensive sampling within these windows. A harmonic potential, $u_i = \frac{1}{2}k(r - r_i)^2$ used as the external biasing potential at window i, where r_i represents the reference location and k denotes the harmonic force constant. We utilized the Weighted Histogram Analysis Method (WHAM) to remove the biasing potential and reconstruct the potential of mean force (PMF).[154] The reaction coordinate, defined as the distance between the centre of mass of gold nucleate and the upper surface of the gold (111) surface was the reaction coordinate. A 1.0 ns production runs were conducted in an NVT ensemble for each window at 303.15 K, employing restraints

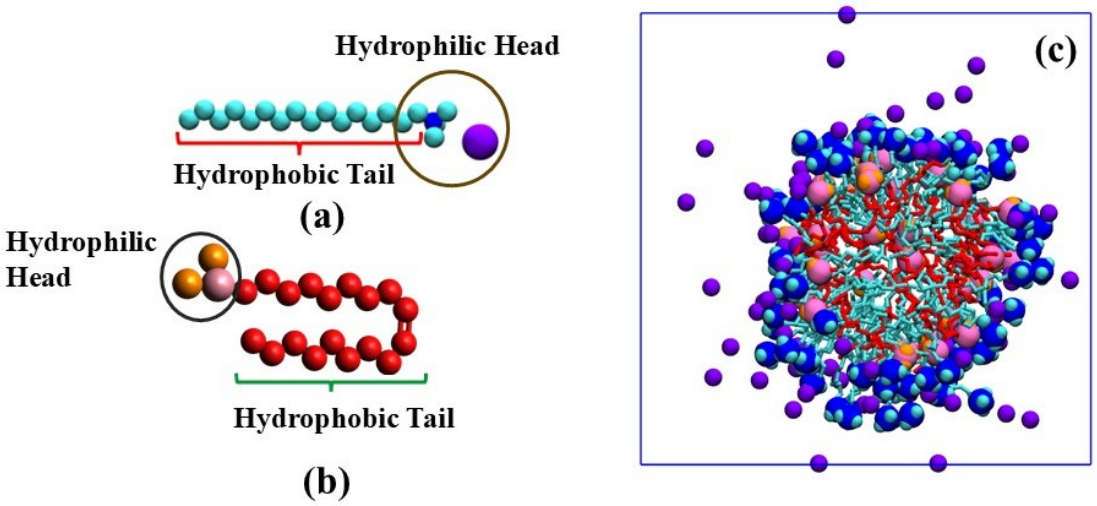

Figure 4.1: Molecular representation of the molecules – (a) CTAB and (b) Oleyamine – indicating their hydrophilic head and hydrophobic tail groups. For CTAB, the methyl groups, nitrogen atoms and bromide ions are represented as cyan, blue and purple spheres, respectively, whereas for oleylamine, the methyl groups, nitrogen atoms and hydrogen atoms are represented as red, pink and orange spheres, respectively; (c) Cross-sectional view of the micelle formed by OLA and CTAB molecules (Molar ratio of OLA/CTAB is 1:2). Water is not shown for visual clarity.

with a harmonic force constant of 100 kcal/mol.Å^2. In WHAM, the calculation of PMF involved setting the number of bins to 100, accompanied by a tolerance for iterations of 10^{-5}. We monitored the size and shape of the micelle by calculating the components of the radius of gyration (R_g) tensor, $R_{g_{xx}}$, $R_{g_{yy}}$, $R_{g_{zz}}$, respectively. The radius of gyration R_g of the micelle was calculated using the equation: $R_g = \sqrt{(\sum_{i=1}^{N}(R_i - R_{COM})^2)/N}$ where, N is the total number of atoms in the micelle, R_{COM} is the center of mass (COM) of that micelle, and R_i is the position of the i^{th} atom in the micelle. We calculated the order parameter to understand the orientation of the molecules within the micelle on the gold surface. The order parameter of the micelle molecules is a measure of the degree of ordering and alignment of CTAB molecules within a micelle structure. The order parameter expressed as $S_{zz} = (3cos^2\theta_i - 1)/2$ where, θ_i is the angle between the end-to-end vector of the i^{th} molecule and the surface normal vector.

4.3 Results and Discussion

We begin by discussing how the cosurfactant OLA, together with CTAB, facilitates the formation of a cylindrical micelle in the solution. To understand the structural properties of the cylindrical CTAB-OLA micelle in solution, we will discuss the changes in some key parameters, such as the density profiles of different components, the radial distribution functions, and the radius of gyration. Quantification of the nucleation process and subsequent engulfment by the micelle will be followed by the estimation of the free energy landscape for a gold nucleate engulfed to adhere to a gold (111) surface will be discussed. In Figure 4.1(c), shows the cross-sectional view of the formed cylindrical micelle by the mixture of the surfactant molecules - OLA and CTAB at a molar ratio of 1:2. It shows the spatial distribution of surfactant molecules within the micelle. This representation further confirmed the structural organization of the molecules, with the hydrophilic CTAB headgroups towards the periphery of the micelles so that they can interact with the surrounding solvent, while the hydrophobic tails of both CTAB and OLA are shielded within the micelle structure. This snapshot depicted that OLA molecules mostly occupy the core of the micelle, while CTAB molecules form the outer shell. This arrangement emphasises the cooperative role of both surfactants, with OLA contributing to the flexibility and stability of the micelle core and CTAB stabilizing the micelle at its periphery.

Figure 4.2a shows the mass density profiles of different components (alkyl chains of CTAB and OLA, ammonium group of CTAB, the amine group of OLA, bromide ions, and water) as a function of distance from the longitudinal axis of the cylindrical micelle at 303.15 K. The density profile of the alkyl chains of CTAB and OLA can be observed at lower distances, indicating that they form the hydrophobic core of the micelle. This is demonstrated by the density profile of these components, with the green triangle representing CTAB and the orange nabla representing OLA. At shorter distances, the alkyl chains of OLA displayed a high density that gradually decreased with increasing distance. In contrast, the density profile of CTAB increased steadily with a distance of approximately 1.5 nm, after which it rapidly declined. This indicated that OLA molecules are more aligned

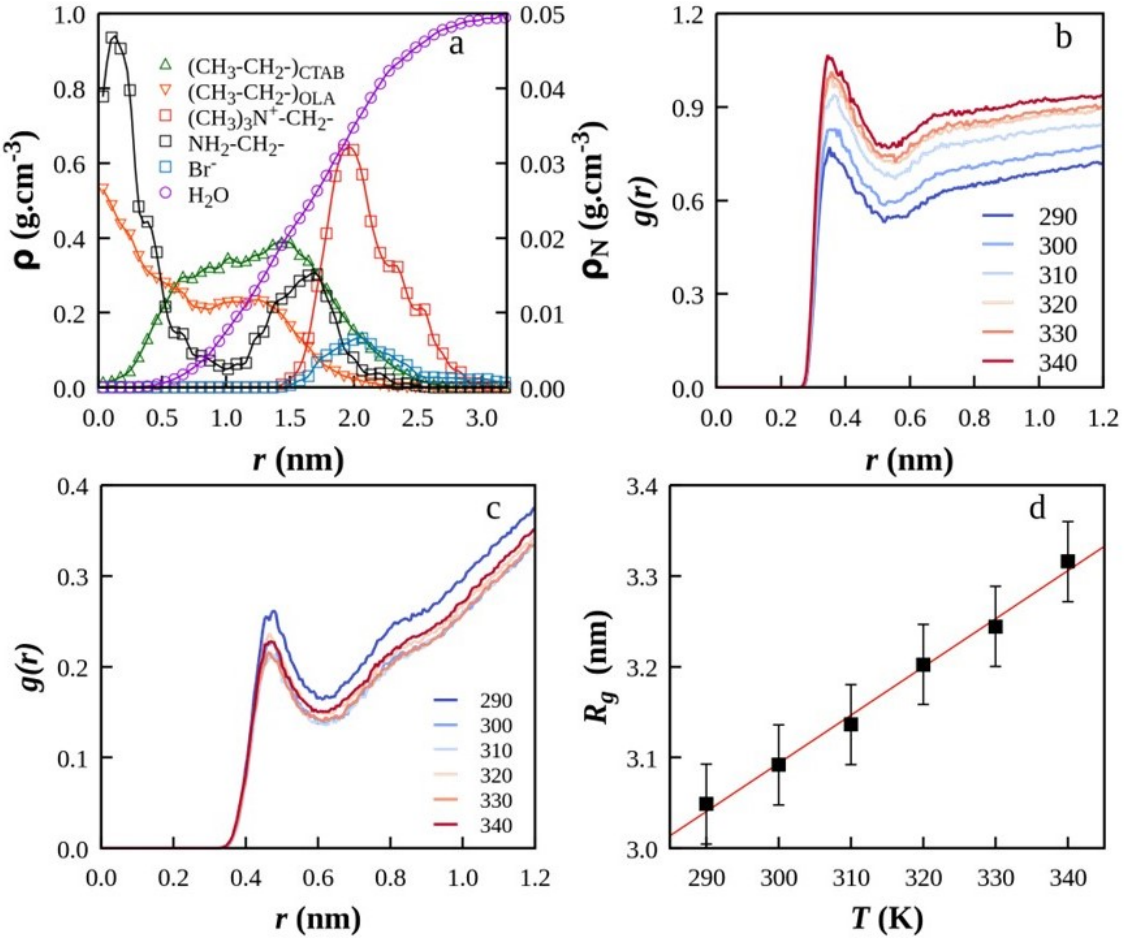

Figure 4.2: (a) Mass density profiles of different segments within the micelle – alkyl chains of CTAB and OLA, ammonium groups, amine groups, bromide ions, and water as a function of distance from the longitudinal axis of the cylindrical micelle at 303.15 K. The right-side scale is for the ammonium and amine groups. (b) Radial distribution functions between the Oxygen in water and N of CTAB molecules at different temperatures; (c) Radial distribution functions between the Oxygen in water and N of OLA molecules at different temperatures; (d) Variation of the radius of gyration of the micelle at different temperatures.

with the longitudinal axis of the cylinder. In spherical micelles, the alkyl chains of CTAB molecules tend to be radially symmetric, whereas in a cylindrical micelle, the alkyl chains align themselves in a plane perpendicular to the longitudinal axis of the cylinder. The gradual decrease of the density profile of alkyl chains of OLA suggested a preferential arrangement of the chains along the longitudinal axis. The sharp peak at ~ 1.95 nm for the ammonium group of CTAB indicated the dimension of the cylindrical micelle radially. The density profile of OLA's amine groups showed a peak inside the hydrophobic core of the micelle, which justifies the arrangement of OLA molecules along the longitudinal axis. The density profile of bromide ions, cf cyan squares, showed that the broader distribution,

as counterions to the positively charged ammonium group of CTAB, is localized near the micelle surface. The density profile of water indicated scarcity of water molecules in the micelle's hydrophobic core, with their density gradually increasing near the hydrophilic headgroups at the micelle surface. Beyond 2.5 nm, water density reached its bulk value.

Figure 4.2b depicts the radial distribution functions (RDFs) between water molecules and the nitrogen atom in the headgroup of CTAB molecules. The peaks at ~ 0.3 nm showed that water formed a solvation shell around the CTAB headgroup, which reflects the strong interaction between the ammonium groups and water molecules, stabilizing the micelle structure. The value of RDF is less than one due to the spatial arrangement of surfactant molecules, in a micelle's core-shell structure, the hydrophobic core may have a lower density of hydrophilic groups. Figure 4.2c shows the radial distribution function between the nitrogen atom of the amine group in the co-surfactant OLA headgroup and surrounding water molecules. The first prominent peak at ~ 0.45 nm represents the formation of a structured solvation shell around the headgroup of OLA. A smaller peak or shoulder after the first peak suggests a less structured, more diffuse second solvation shell. Figure 4.2d shows the change in the radius of gyration of the micelle at different temperatures, indicating that the micelle suffered an expansion with the increase in temperature. At higher temperatures, increased thermal motion can reduce the organisation or clustering of particles, leading to a lower RDF value at specific distances. Here, in this case, R_{gxx} and R_{gyy} are dominating, which suggests that the expansion is anisotropic, with the micelle elongating along specific directions. This could be due to the alignment or orientation of surfactant and co-surfactant molecules in response to the thermal effects, leading to a deformation of the micelle from a more spherical shape to an elongated or rod-like structure. However, we were keen to understand the growth of gold nucleates from the solution.

Figure 4.3a shows snapshots of the engulfing of gold nucleates by the cylindrical micelle in solution at 60 ns. The formed gold nucleate is elliptical in shape, which suggests that the growth along one axis was more favourable compared to other directions. This could be due to the potential alignment of surfactant molecules, which could guide the gold atoms preferentially in a specific direction. Figure 4.3b shows the evaluation of the number of

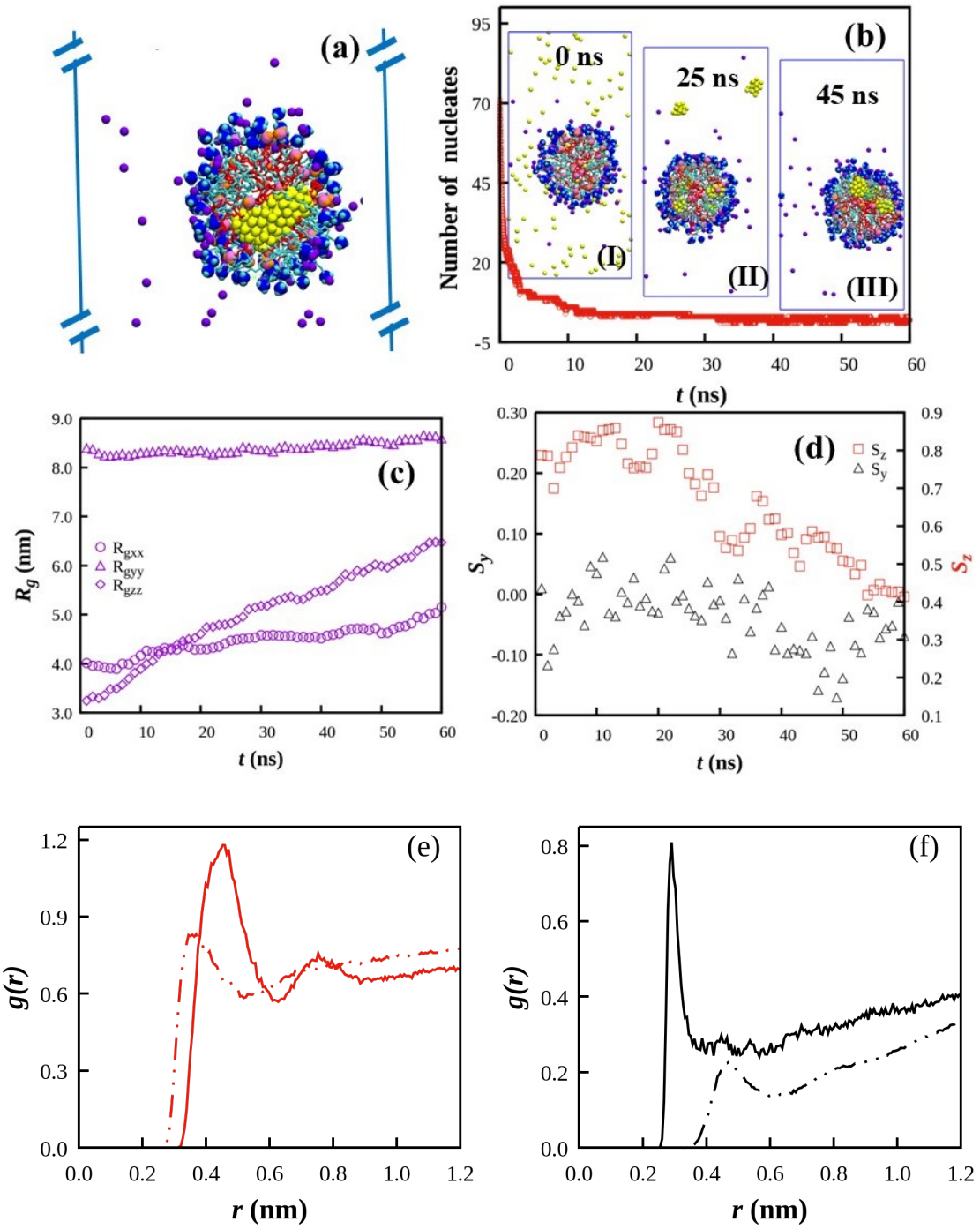

Figure 4.3: (a) Formation of Gold nucleates inside the micelle in solution. (b) Formation of the number of nucleates as a function of time; Insets (I-III) contain the snapshots of nucleate formation at 0, 25 and 45 ns. (c) The radius of gyration of micelle with time. (d) The change in order parameter of OLA molecules in the y-direction (left axis) and CTAB molecules in the z-direction (right axis). Colour codes for molecular presentation are the same as in Figure 4.1; water is omitted for visual clarity. (e,f) Comparison of RDFs between the head group of surfactant molecules (red: CTAB and black: OLA) and water molecules after engulfing nucleates (solid lines) and that of a pure micelle (dashed line), respectively.

nucleates with time. The exponential decay in the number of nucleates, followed by stabilization, indicated a transition from an initial nucleation-dominated regime to a growth and coalescence regime where nucleates merge to form larger clusters. The entire process can be divided into three parts – $first$, initially, as shown in Inset I, 100 gold atoms dispersed throughout the aqueous solutions, mimicking the random reduction of the precursor molecules to Au atoms; $second$, at $\sim$ 25 ns, a transition stage, shown in an Inset II, where several gold nucleates have formed, indicating the gold atoms are aggregating; and $third$, the final stage of nucleation, $\sim$ 45 ns when fewer numbers of larger nucleates are formed by coalescences of smaller nucleates into larger aggregates, shown in Inset III. We calculated the different components of the radius of gyration, i.e. $R_{g_{xx}}$, $R_{g_{yy}}$, and $R_{g_{zz}}$. In Figure 4.3c, the positive slopes for $R_{g_{xx}}$ and $R_{g_{zz}}$ with time can be observed. It revealed that the micelle swelled in the xz-plane to accommodate the growing gold nucleates. This expansion along the xz plane can significantly influence the growth kinetics for nucleation inside the micelles. To see the changes in the structure of the cylindrical micelle, we have calculated the order parameter (S_z) of the surfactant molecules and represented its changes with time in Figure 4.3d. The left and right Y axes are used to scale the order parameters of OLA and CTAB molecules, respectively. First, we focus on the changes in the order parameter of the CTAB molecules, which is calculated with respect to the z axis. At the beginning, the S_z values fluctuate till $\sim$25 ns. This is the time in which most of the atoms are percolated to the core of the micelle. Beyond this point, the atoms start to form larger nucleates inside the micelle, and the molecules keep changing their arrangement to accommodate the changes in the nucleate structure.

Further, we have calculated the order parameter of the OLA molecules in the y-direction on the left axis. Initially, it shows a negative value, which indicates that OLA molecules are significantly more disordered than CTAB. Unlike CTAB, the S_y of OLA remains consistently low throughout the process, fluctuating between -0.2 and 0.1. This suggests that OLA molecules do not achieve significant alignment, even as nucleation progresses. We observed that the maximum value of S_y for OLA remains below 0.1, emphasizing that OLA molecules are largely disordered and do not form a well-aligned structure. The S_y

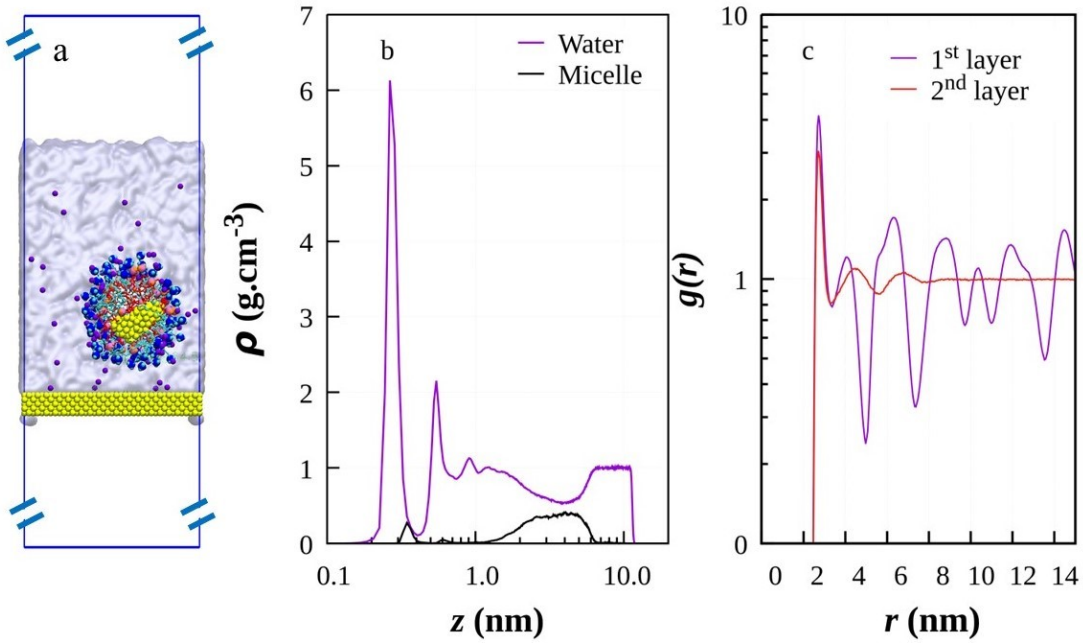

Figure 4.4: (a) Snapshot of the nucleate engulfed cylindrical micelle of CATB-OLA surfactants away from the gold surface in an aqueous media. The Au(111) surface, at the bottom, is represented in yellow spheres. Water has shown an ice-blue colour in continuous media. The blue rectangle represents the periodic box (not to scale in the z-direction). (b) Mass density of water and micelle as a function of distance from Au(111) gold surface. (c) In-plane pair correlations between water molecules in the layer adjacent to the Au(111) gold surface.

for OLA showed minor fluctuations, but there is no clear trend of increasing alignment as observed for CTAB. This could be due to the dynamic interaction of OLA with CTAB and the surrounding water, which disrupts its ordering. In order to understand the nucleation process, we focus on the nucleation of the gold atoms in the presence of the micelles. Figure 4.3(e,f) indicates micelles after engulfing nucleates have a higher RDF peak value (solid lines) compared to a pure micelle (dashed lines). This suggests that nucleate incorporation does not displace water but instead alters the micelle structure in a way that enhances hydration. The nucleates may increase the accessibility of surfactant head groups to water, possibly by expanding the micelle structure or altering its curvature. If micelle deformation occurs, it might expose more head groups to the solvent, leading to higher water density near the interface. A shift in peak position (right to left) in Figure 4.3(f) suggests a change in hydration structure.

The cylindrical micelle with engulfed gold nucleates was far from the surface, as shown

in Figure 4.4a; we observe that a nucleate-engulfed micelle remains stable in an aqueous solution – away from the surface. After 60 ns simulations, it did not migrate to the surface, indicating the presence of an energy barrier. It is crucial to identify the cause behind this energy barrier that prevents the micelle from approaching the surface. For the quantification of the energy barrier, we performed a series of biased simulations constraining the position of the micelle by a harmonic potential. The potential of mean force was calculated by applying the weighted histogram analysis method (WHAM). The energy barrier arises primarily due to the strong layering of water molecules on the Au(111) gold surface. To understand the behaviour of the water layer near the surface, we calculated the density profile and the radial distribution functions. Figure 4.4 (b) depicts the density profiles of different components of the solution, i.e. water and micelle, as a function of distance from the surface, providing insight into their spatial distribution in the simulation system. The sharp peak represented by the purple line near the surface (at $\sim$0.2 nm) indicated a high-density layer of water molecules strongly adsorbed onto the gold surface, and a subsequent peak at $\sim$0.5 nm. Beyond these peaks, the water density gradually reached a constant value indicative of the bulk water phase. The micelle density profile, represented by the black line, showed its position in the liquid zone, peaked at ~ 2.4 nm, corresponding to the micelle's equilibrium position relative to the gold surface. This interaction contributes to the hydration layer's stability and influences the micelle's structural integrity and behaviour in the aqueous medium. These two strong layers need attention, and we have looked into their structural properties by calculating the in-plane radial distribution functions and showing them in Figure 4.4(c). The first layer of water molecules showed periodic sharp peaks in its in-plane RDF, indicative of a solid-like repetitive structure. It indicated a strongly ordered arrangement of water molecules near the gold surface due to strong adsorption and surface interactions. This ordered structure corresponds to the dense water layer that created the energy barrier for the micelle, as discussed in Figure 4.4(b). The second strong peak in the water density profile, shown in Figure 4.4b, is observed at ~ 0.5 nm), the 2^{nd} layer of water molecules on the surface, demonstrated a less-ordered but structured hydration layer as indicated by sharp first peak

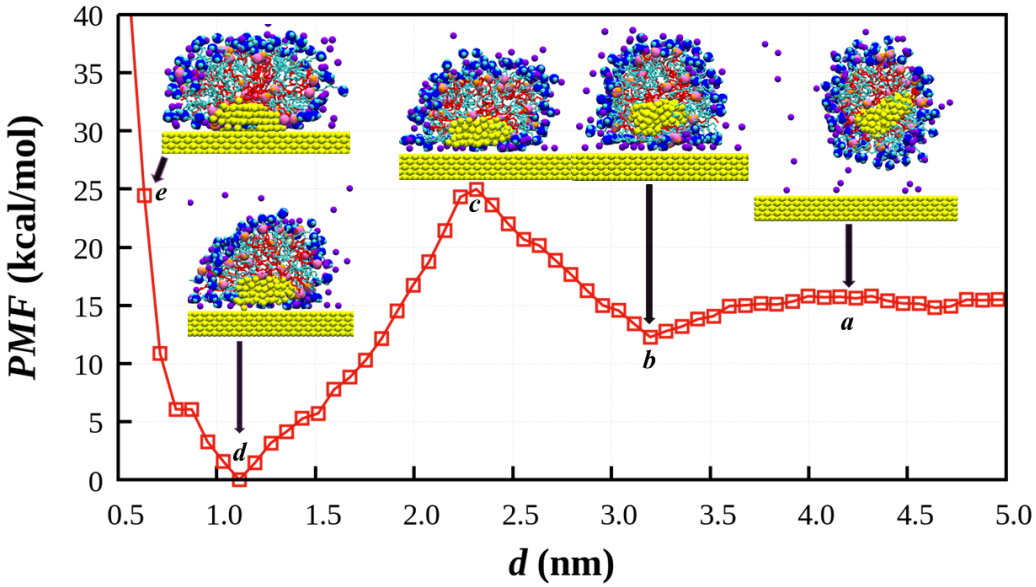

Figure 4.5: Potential of mean force between the centre of mass of gold nucleate and the top of the gold (111) surface. Snapshots inside the plot show the relative positions of nucleate and micelle on the surface. The black arrows indicate the position of the nucleate from the apex of the gold surface. The colour codes for molecular presentation are the same as in Figure 4.1, and water is omitted for clarity.

and quick damping of it in the in-plane radial distribution function, Figure 4.4c. In order to quantify the barrier, we have estimated it using the potential of mean force.

In Figure 4.5, we have shown the potential of the mean force for the nucleate towards the surface through the solution. The micelle-nucleate assembly was stable at a distance of 4-5 nm from the surface. As the assembly was pushed towards the surface, it experienced an energy barrier, as indicated by point c in Figure 4.5. Beyond this point, the assembly experienced a much favourable energy landscape and reached the bottom of the valley. As the nucleate resides in the cylindrical micelle, composed of co-surfactant OLA and CTAB, away from the gold surface, as shown in Figure 4.5, it forms a more stable state (i.e., higher energy state, "a" in Figure 4.5). As the micelle containing gold nucleate moves towards the surface, there is a slight drop observed at ~ 3.2 nm (point "b"), indicating a lower energy state. This decrease can be attributed to initial weak interactions between the micelle and the gold surface, leading to the structural arrangement of the molecules within the micelle. As the micelle approaches the surface further, the PMF increases significantly, indicating an energy barrier. This is due to the reorganisation of surfactant molecules within the

micelle – exposing nucleate to the solvent molecules and the breaking of water-mediated interactions between the gold surface and the gold nucleate-infused micelle. Once the micelle passes the energy barrier, it begins to flatten and make closer contact with the surface. This leads to a significant decrease in the PMF, reaching its minimum at ~ 1.2 nm (point "d"), where the system is in the most stable configuration. Moreover, the micelle molecules were trying to rearrange themselves towards another micelle, which was prevented by the strong affinity of gold atoms and micelle molecules. The co-surfactant, however, brought deformability to the cylindrical micelle during the nucleation. This deformation aids in releasing the gold nucleate onto the gold surface, facilitating nucleation. Further, the energy increases (point "e") due to the breaking of the gold nucleate on a gold surface. This study aims to understand the growth of gold nanocrystals on the gold surface with co-surfactant OLA and surfactant CTAB. When the gold nucleate was pushed towards the surface, the micelle was deformed, and a few OLA molecules came out of the micelle and resided on the surface. Further, a few CTAB molecules are adsorbed on the surface, which increases the PMF as indicated by a steep line in Figure 4.5.

We have shown the top view and side view of micelle containing gold nucleate in Figure 4.6a and 4.6b. It provided a detailed visual representation of how micelle structure changes when interacting with gold nucleate, especially in the presence of a gold surface. The top view showed that the micelle can deform significantly to accommodate the nucleate. In side view (Figure 4.6b), it is apparent that the micelle becomes elongated or deformed near the gold nucleate, possibly due to the interaction of nucleate with the gold surface. This deformation is necessary to accommodate the growing nucleate while maintaining stability. To determine the micelles' deformation, we have calculated the order parameter and radius of gyration with the distance between the centre of mass of gold nucleate and the surface as shown in Figure 4.6c. When the gold nucleate-infused micelle is far from the surface (~ 5 nm), S_{zz} decreases, indicating a loss of alignment and a transition to a more disordered state. Further, the drop is observed at ~ 4 nm which signifies a transitional region where the micelle begins to lose its orientational order along the z-axis, signalling a structural reorganization driven by the diminishing influence of the surface. However, as

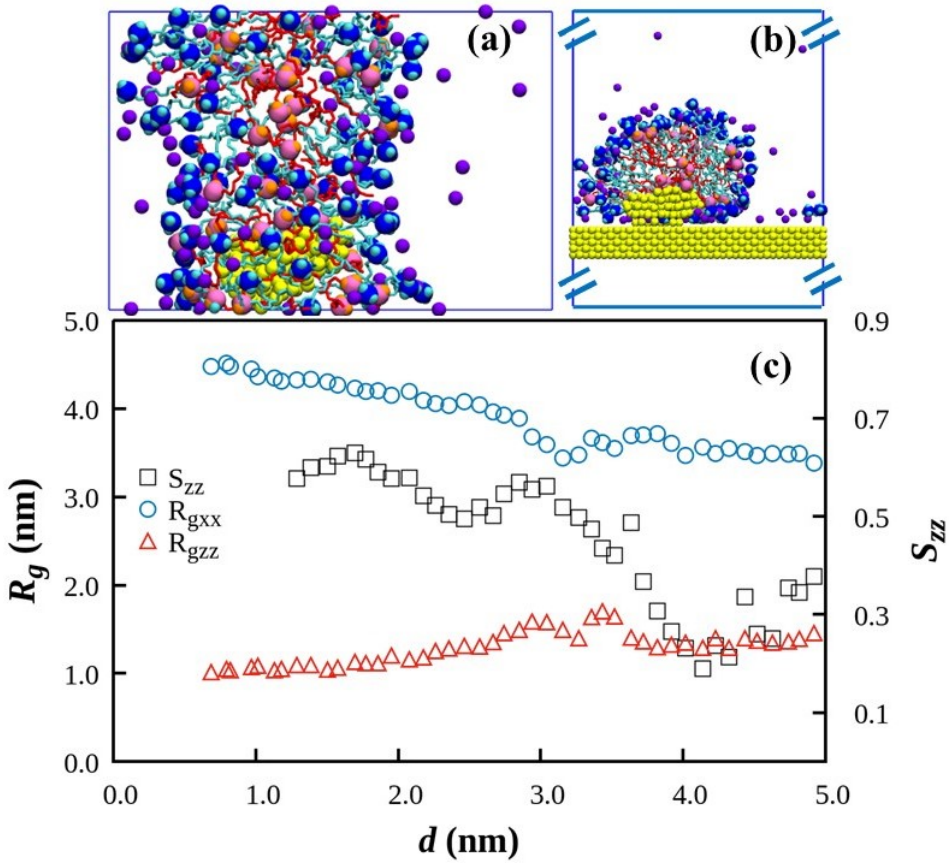

Figure 4.6: The top view and side view of a micelle containing nucleate are shown in (a) and (b), respectively. The colour codes for molecular presentation are the same as in Figure 4.1; the gold surface and water molecules are omitted for clarity. (c)The change in order parameter (right axis) and radius of gyration (left axis) of the micelle with distance between the centre of mass of gold nucleate and the top of the gold (111) surface.

the micelle moves closer to the surface, S_{zz} increases, indicating a regain in orientational order due to stronger surface interactions, such as electrostatic forces or hydrogen bonding, which align the molecular components. Similarly, the radius of gyration components revealed structural changes. It indicated that the micelle became increasingly elongated in the x and z directions.[156]

4.4 Summary

This study summarized that the growth of gold nanocrystals is significantly influenced by the presence of co-surfactant OLA alongside the primary surfactant CTAB. The co-surfactant OLA plays a pivotal role in reducing the free energy required for the cylindrical micelle to reach and interact with the gold surface, compared to a single CTAB micelle.

As shown in Figure 4.5, the micelle achieves greater stability on the surface than in bulk, emphasizing the importance of micelle-surface interactions.

The free energy landscape constructed through molecular dynamics simulations revealed a high energy barrier (~ 10.36 kcal/mol) for gold nucleates breaking free from a micelle composed solely of CTAB surfactant. However, the inclusion of OLA facilitates micelle deformation and structural adaptation, which is critical for releasing gold nucleates onto the surface. The most stable configuration occurs at a distance of 1.2 nm, where strong micelle-surface interactions stabilize the system. Additionally, the adsorption of OLA and CTAB onto the surface increases the PMF, reflecting the complex interplay of forces governing nanocrystal growth.

This study provides critical insights into the molecular mechanisms of nucleation and growth, emphasizing the role of micelle deformation and surfactant alignment in overcoming energy barriers. The findings highlight the potential of co-surfactant systems to tailor micellar properties for controlled nanomaterial synthesis, offering valuable strategies for optimizing processes in nanotechnology, drug delivery, and material science. These findings offer a pathway for advancing nanomaterial synthesis, surface functionalization, and applications in drug delivery and nanotechnology.